

Petrogenesis of the Chagangnuoer deposit, NW China: a general model for submarine volcanic-hosted skarn iron deposits

Wenli Sun · Yaoling Niu · Yuxin Ma · Yi Liu · Guorui Zhang ·
Zhenxing Hu · Zhaowei Zhang · Shuo Chen · Jiyong Li ·
Xiaohong Wang · Hongmei Gong

Received: 4 August 2014 / Accepted: 8 October 2014 / Published online: 20 January 2015
© Science China Press and Springer-Verlag Berlin Heidelberg 2015

Abstract The Chagangnuoer deposit is a typical submarine volcanic rock-hosted skarn iron deposit, where orebodies mainly occur in andesitic rocks of the Dahalajunshan Formation (DF) with skarns well developed around orebodies. The volcanic rocks of the DF in the Chagangnuoer deposit display calc-alkaline characteristics. The ore-bearing andesitic rocks have high $^{87}\text{Sr}/^{86}\text{Sr}_{(i)}$ (0.7058–0.7117) and low $\varepsilon_{\text{Nd}}(t)$ (–3.51 to 1.67). They probably formed through mixing of basaltic melts and the induced crustal melts. LA-ICP-MS U–Pb zircon ages of 250 and 305 Ma are obtained for the granite and granodiorite in the Chagangnuoer deposit, respectively, which are significantly younger than the timing of the skarn formation

(316 Ma). These age data indicate that the granitoids have no contribution to the skarn and associated iron mineralization. This paper proposes a new genetic model for submarine volcanic rock-hosted skarn iron deposits, in which the iron mineralization, skarn formation and volcanic magmatism are necessary aspects of the same system; the iron separates and concentrates from the silicate magma in the form of Fe(II) carbonate complex. While this conceptual model is largely based on observations on the Chagangnuoer deposit, it may have general significance for skarn-type iron deposits associated with submarine volcanic rock sequences and warrants further testing and improvement.

Electronic supplementary material The online version of this article (doi:10.1007/s11434-014-0684-9) contains supplementary material, which is available to authorized users.

Keywords Volcanic rocks-hosted skarn iron deposit · Petrogenesis of ore-bearing andesitic rocks · U–Pb zircon ages · New genetic model

W. Sun (✉) · Y. Ma · G. Zhang · Z. Hu
School of Earth Sciences, Lanzhou University, Lanzhou 730000,
China
e-mail: 13619335704@163.com

W. Sun · Y. Niu (✉) · S. Chen · J. Li · X. Wang · H. Gong
Institute of Oceanology, Chinese Academy of Sciences, Qingdao
266071, China
e-mail: yaoling.niu@foxmail.com

W. Sun
Gansu Industry Polytechnic College, Tianshui 741025, China

Y. Niu
Department of Earth Sciences, Durham University, Durham
DH1 3LE, UK

Y. Liu
China University of Geosciences, Beijing 100083, China

Z. Zhang
Xi'an Center of Geological Survey, Xi'an 710054, China

1 Introduction

Submarine volcanogenic iron oxide (SVIO) ore systems mainly include volcanic-associated and (volcano sedimentary)-hosted iron deposits. Many of these deposits are characterized by well-developed skarn assemblages, such as the Chagangnuoer, Anzas, Tuomuerte, Dundee, Yamansu and Beizhan iron deposits [1–8]. In these deposits, skarn rocks and orebodies occur in specific volcanic rock formations and lack clear link with intrusive rocks in time and space; these deposits are thus inconsistent with conventional intrusion-related skarn deposits with characteristic features including spatial zonation of skarn mineral assemblages and proximity to contacts with igneous intrusions. These skarns could be interpreted as a distal expression of magmatic activity [8–10]. Some researchers suggested that later hydrothermal alteration might have led to the skarn

formation and their associated mineralization [2, 11, 12]. However, geochronological data indicate that the skarn formation and magmatism of the volcanic rocks are coeval in most cases, such as the Chaganguoer deposit in western Tianshan [13–15] and the Yamansu deposit in eastern Tianshan [8]. Therefore, it is logical to infer that the ore genesis and the skarn development must be genetically related to the evolution of magmatic-hydrothermal fluids derived from the exhalation of coeval submarine volcanism or deep intrusion [7–10, 16]. The fluids could travel some distance from their source to interact with appropriate country rocks (Ca-rich volcanic rocks and/or carbonates) to generate skarns [8, 16]. However, the mechanisms of skarn formation and associated metallogenesis in these models remain ambiguous and controversial, e.g., how iron actually aggregates and precipitates is unclear. Some researchers proposed the concept of “deep skarn environment”, where skarns were thought to develop at magma/wall-rock contacts beneath volcanoes [17–19], and hence the associated metallogenesis [20–24]. They envisaged that deep magma assimilated limestone and underwent subsequently immiscible separation of iron-enriched ore melt. However, what may have led to ore melt immiscibility is still an enigma.

The eastern Awulale Metallogenic Belt (AMB) in western Tianshan is one of the important Chinese SVIO-metallogenic provinces [25] (Fig. 1), in which several iron deposits have been discovered or explored, such as Chaganguoer, Zhibo, Beizhan, Dundu, with more than 1.2 billion tons iron ores [29] (Table 1). All these deposits (Table 1) occur in the Dahalajunshan Formation (DF) which is predominantly composed of basalt, trachyte, trachyandesite, andesite, rhyolite, tuff, volcanoclastic sedimentary rocks, and sandstone and limestone [30]. The Chaganguoer deposit is one of the major iron deposits, where orebodies occur mainly in the andesitic rocks of DF and skarns develop pervasively around the orebodies [29] (Fig. 1b). Recent studies have shown that the iron deposit formed in the later Carboniferous [4] and the volcanic rocks of DF in the eastern AMB in this special time displayed an arc-affinity [7, 10]. The basaltic rocks are derived from depleted mantle [30], and the skarn mineralogy characteristics in this deposit are consistent with typical skarn iron deposits [4]. The above understandings are important. However, (1) the petrogenesis of ore-bearing andesitic rocks is poorly understood; (2) the suggested link between iron mineralization and granitoids in the ore district is unverified; and (3) the origin of the skarns and their associated iron mineralization in the Chaganguoer deposit, like other such deposits elsewhere, is currently controversial.

In this paper, we report new petrological, geochemical and geochronological data for the host rocks, with which we discuss the petrogenesis of ore-hosting andesitic rocks in the DF, and propose a new genetic model for the submarine volcanic-hosted skarn iron deposit, which may prove to be of general significance.

2 Regional geology

The Tianshan orogenic belt in northwestern China is located in the southern part of the Central Asian Orogenic Belt, which is divided into Western and Eastern Tianshan Belts [33–35]. The Western Tianshan Belt comprises four segments, including the North Tianshan arc accretionary complex, the Yili block, the central Tianshan arc terrane and the northern margin of the Tarim block [36]. The Western Tianshan Belt has undergone a complex tectonic evolution before Phanerozoic eon, including accretion and breakup of Pangea and Rodinia supercontinents. In the early Paleozoic, its tectonic setting may belong to multi-continental blocks and multi-island arcs. It may have resulted from the closure of three Paleozoic oceans (the Terskey, North Tianshan and South Tianshan oceans) and the related amalgamations of micro-continents during the Late Paleozoic [36, 37]. Although the ocean closing time is in debate, the Western Tianshan Belt evolved into the post-collisional evolution stage in the Permian [36].

Recently, many significant Fe–Cu–Mo–Au deposits have been recognized and evaluated in the western Tianshan. The Awulale Metallogenic Belt (AMB) in the northeast of Yili block is one of the major iron ore mining areas (Fig. 1b). The Yili block is a triangular-shaped terrain. During the subduction of the North Tianshan and South Tianshan seafloors, Late Devonian to Carboniferous arc magmatism produced a number of volcanic and intrusive complexes in the Yili block [5–7, 10]. The Carboniferous volcanic activities in the AMB have a close spatial–temporal relationship with the iron deposits.

The AMB displays numerous E–W-striking, north-dipping high-angle faults and a synclinal structure [10]. Remote sensing image data show that there is a caldera structure in the AMB [15]. The AMB has a Precambrian basement dominated by Meso- to Neo-Proterozoic gneisses, marble, migmatite and clastic rocks [15, 38, 39]. Silurian volcano sedimentary rocks and Devonian volcanoclastic sedimentary rocks outcrop along the northern and southern margins of the AMB. Limestones of Silurian and Devonian ages develop well in the Chaganguoer deposit [15]. The Carboniferous volcanic and volcanoclastic rocks are widely distributed in the AMB as a result of slab subduction [40]. Most iron deposits are confined within the Carboniferous Dahalajunshan Formation, where ~300 m limestone exist [14]. The Permian, Triassic and Jurassic strata locally occur and mainly consist of conglomerate, sandstone, mudstone and shale [15]. Cretaceous strata are lacking. Quaternary sediments are exposed in the southern margin. There are large volumes of Permian granitoids in the AMB.

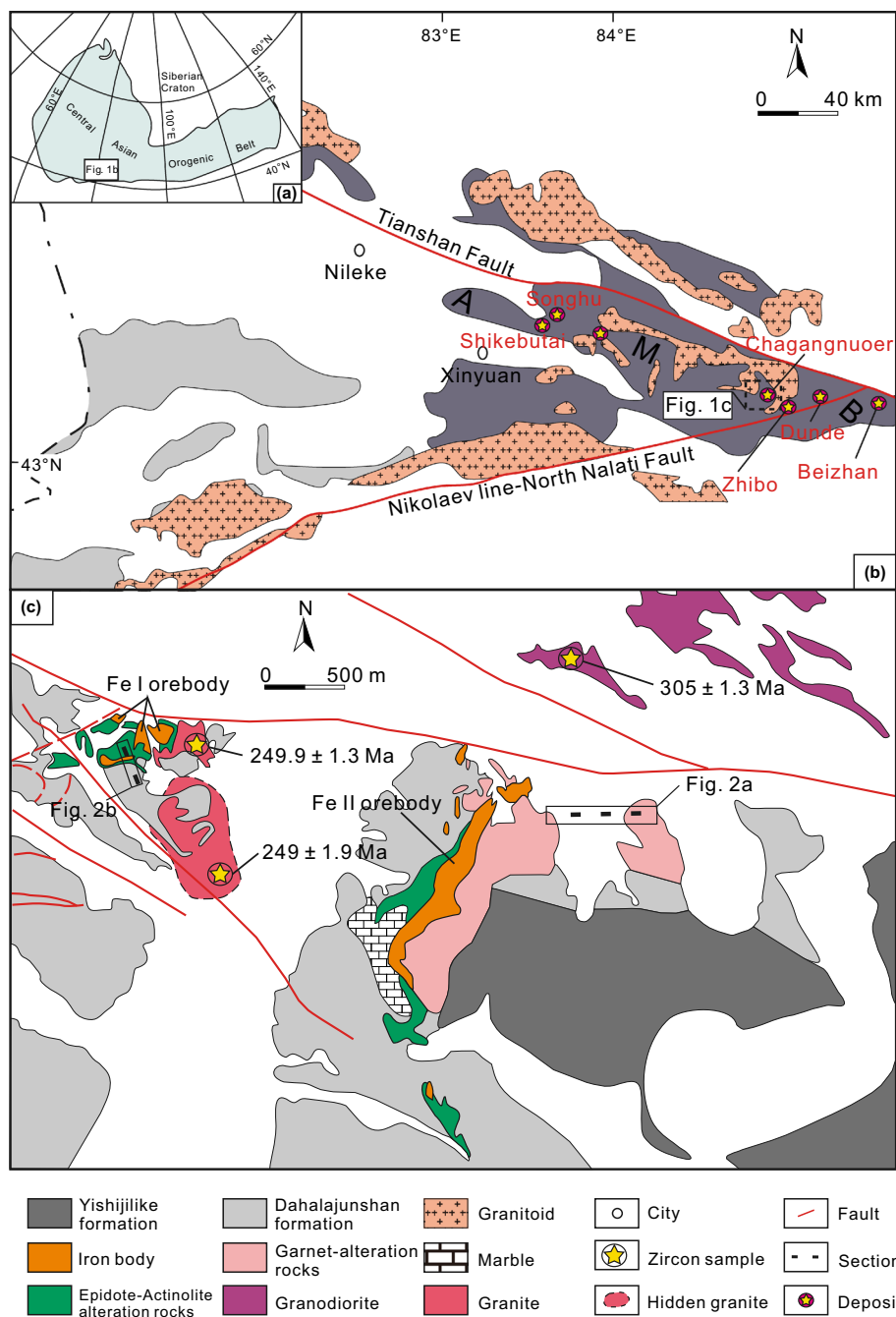


Fig. 1 (a) Tectonic sketch map of the Central Asian Orogenic Belt (modified after Han et al. [26] and Xiao et al. [27]); (b) The iron ores deposits in Awulale Metallogenetic Belt (AMB) (modified after Jiang et al. [28]); and (c) Geological map of the Chagangnuoer iron ore deposit (c after Zhang et al. [14])

3 Local geology

The Chagangnuoer iron deposit is located in the eastern segment of the Awulale Metallogenetic Belt (Fig. 1b), and the iron reserve exceeds 200 million tons. The Carboniferous Dahalajunshan Formation (DF), Yishijilike Formation, granitoids and Quaternary sediments are exposed in the ore

district (Fig. 1c). Granitoids develop in the northeastern part and granite crops out east of Fe I ore body (Fig. 1c). Recently, hidden amonzonitic granite is found in the south of Fe I orebody with mafic magmatic enclaves.

Six orebodies have been recognized and they occur mainly in andesitic rocks of the DF. The orebodies are mostly tabular or lenticular (Fig. 2). Fe I orebody and Fe II

orebody are economically large (Fig. 1c). The average ore grade of Fe II orebody is 37 % and 33 % in Fe I orebody.

The skarns are very common in the Chagangnuoer deposit, where progressive skarnization such as garnet, diopside, actinolite and retrogressive alteration such as chlorite, epidote, sulfides, silica and calcite are well developed around ore bodies. As shown in Fig. 1c, from east to west of Fe II orebody, garnet alteration zone, actinolite alteration zone and marble alteration zone are well defined. The borehole samples show that there exist garnet alteration, epidote-actinolite alteration, epidote-diopside alteration and marble around iron bodies (Fig. 2). Hong et al. [3] subdivided the deposit into magnetite-diopside stage, chlorite-pyrite stage, magnetite-garnet-actinolite stage, epidote-chlorite stage, sulfide stage and quartz-carbonate stage.

The ore minerals are magnetite and hematite. The major gangue minerals are garnet, diopside and epidote plus minor actinolite, chlorite, plagioclase, quartz and carbonate. Eight types of ores have been recognized by Feng et al. [15], of which the most important is brecciated ores (Fig. 3a, e). Ore textures are dominated by xenomorphic-hypidiomorphic granular and auto-hypidiomorphic granular.

4 Samples

A total of 14 samples (6 andesitic rock samples and 5 granodiorite samples and 3 iron ore samples) have been analyzed for major and trace elements. The six andesitic samples have been analyzed for Sr and Nd isotopes, and their rock types and petrography are summarized in Table 2, which includes descriptions of two iron ore samples and two granodiorite samples. Three intrusive rock samples were chosen for zircon LA-ICP-MS U–Pb age dating. The geochemical data on these samples and other samples in the literature [10, 15, 28, 30, 41] are used for discussion.

5 Analytical techniques

Bulk rock major and trace element analysis of volcanic rocks and iron ores (Table 3) were conducted at the State Key Laboratory of Geological Process and Mineral Resources of the China University of Geosciences, Beijing (CUGB). Major elements were determined using Leeman Prodigy inductively coupled plasma-optical spectroscopy (ICP-OES) system with high dispersion Echelle optics. Precisions for most major elements based on rock standards BCR-1, AGV-2 [US Geological Survey (USGS)] and GSR-3 (national geological standard reference materials (SRM) of China) are better than 1 % with the exception of

Table 1 Geological characteristics of major iron deposits in the eastern AMB

Deposit name	Ore-bearing rocks	Rock formation	Scale	Wall-rock alteration	Shape of orebodies	U–Pb age	References
Chagangnuoer	Andesite, andesitic volcanic rocks	Dahalajunshan Formation	Large	Skarn alteration	Layer, lentiform	305 Ma for granodiorite 301 and 321 Ma for rhyolite	This study, [28, 30]
Zhibo	Basaltic andesite andesitic tuff		Large	Ca, K, Na metasomatism	Lens, tabular	300 Ma for dacite, 329 Ma for andesite, 304 Ma for granite, 319 Ma for diorite	[14, 28]
Dunde	Dacite, basaltic tuff, andesitic tuff		Medium	Skarn alteration carbonatization alteration epidotization	Lens, layer	316 Ma for dacite	[7]
Beizhan	Dacite, calcareous shale, dolomite		Large	Skarn alteration, carbonatization alteration	Layer, lentiform	301 Ma for rhyolite 303 and 329 Ma for dacite	[31, 32]

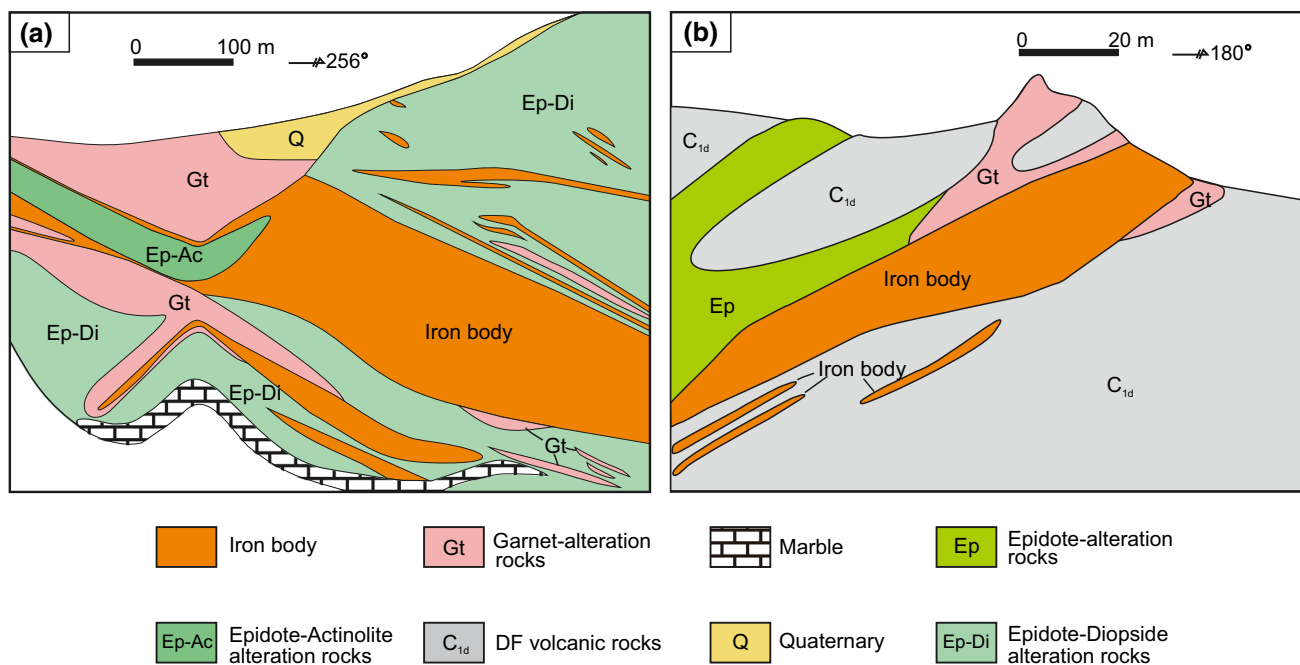


Fig. 2 Cross sections illustrate the skarn alteration phenomena of host rocks in the Chaganguoer mine. Both of **a** and **b** are modified from Feng et al. [15]

TiO₂ (1.5 %) and P₂O₅ (2.0 %) (see [42] for analytical details). Trace elements were analyzed using ICP-MS after Teflon bomb-assisted total acid digestion and dilution (see [42] for analytical details). Sample was dissolved in equal mixture of subboiling distilled HF and HNO₃ with a Teflon digesting vessel on a hot plate for 24 h using high-pressure bombs to ensure complete digestion/dissolution (see [42] for analytical details).

Sr was analyzed using TIMS and Nd isotope by Neptune Plus MC-ICP-MS at the State Key Laboratory of Geological Process and Mineral Resources of the China University of Geosciences, Wuhan (CUGW) (Table 4). About 100 mg samples were digested in a Teflon bomb with a mixture of concentrated HNO₃ and HF. The sealed bombs were kept in an oven at 190 °C for 48 h. The decomposed samples were then dried on a hot plate and converted into chlorides by adding one milliliter of 6 mol/L HCl, followed by a final evaporation. The samples were dissolved again in 1 mL of 2.5 mol/L HCl and then centrifugated. The final solutions were used for separating and purifying elements Sr and Nd by means of ion exchange columns of Dowex AG50WX12 cation resin and Eichrom Ln-Spec resin successively.

U–Pb dating and trace element analysis of zircons were done simultaneously using LA-ICP-MS at the State Key Laboratory of Geological Processes and Mineral Resources, China University of Geosciences (CUGW) (Table S1). Laser sampling was conducted using a GeoLas 2005

System with a spot size of 32 μm. An Agilent 7500a ICP-MS instrument was used to acquire ion-signal intensities (see [43, 44] for analytical details).

6 Results

6.1 Geochronology

Three granitoid samples were chosen for LA-ICP-MS U–Pb zircon analyses. The data are listed in Table S1.

In sample CGNE12-01, most zircon grains are euhedral with a clear oscillatory zoning (Fig. 4). The Th/U ratio of the analyzed grains varies from 0.40 to 0.72. These characteristics indicate a magmatic origin [45, 46]. All of the seventeen analyzed spots cluster on the concordant and yield a weighted mean ²⁰⁶Pb/²³⁸U age of 249.9 ± 1.3 Ma (MSWD = 0.13) (Fig. 5a).

In sample CGNE12-05, all the zircon grains are colorless and subhedral with blurred oscillatory zoning (Fig. 4). They are 90–110 μm in length with length to width ratios of 1.5:1 to 3:1. All of the sixteen analyzed zircon grains cluster on the concordant yielding ²⁰⁶Pb/²³⁸U ages between 247 and 260 Ma, giving a weighted mean ²⁰⁶Pb/²³⁸U age of 249 ± 1.9 Ma (MSWD = 1.4) (Fig. 5b).

In sample ZK06-830, all zircon grains are colorless. They are subhedral, stubby prismatic crystals with length to width ratios of 1.1:1 to 1.5:1. All the grains exhibit well-

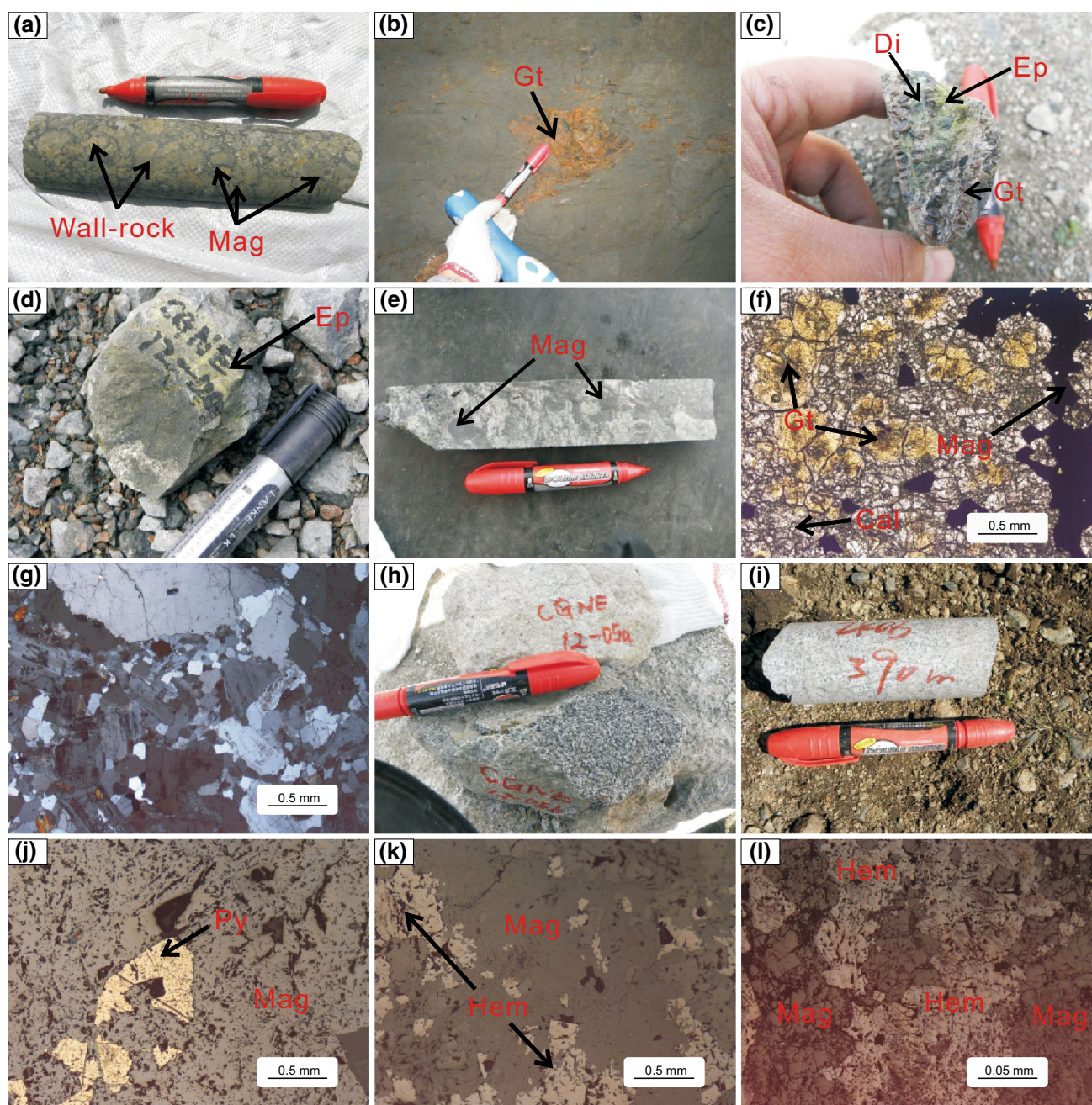


Fig. 3 Ore feature and granitoids from Changanuoer deposits. **a** brecciated ores in which breccias are magnetite cemented by altered mineral, **b** garnet in Changanuoer 3001 adit, **c** garnet, epidote and diopside, **d** epidote alteration, **e** brecciated ores in which breccias are debris cemented by magnetite, **f** calcite was altered and formed garnet, **g** micrograph of CGNE12-01 granite, **h** CGNE12-05 granite, **i** granodiorite exposed in the northeastern of ore district, **j** pyrite and magnetite, **k** magnetite and hematite, **l** magnetite and hematite. Gt, garnet; Ep, epidote; Di, diopside; Cal, calcite; Mag, magnetite; Hem, hematite

developed oscillatory zoning (Fig. 4). The Th/U ratios for analyzed grains vary from 0.42 to 0.86 (Table S1), higher than those of metamorphic zircon grains (<0.2) [46, 47], indicating a magmatic origin. Except for analyses at spots of the cores, all the 18 analyzed spots yield a weighted mean $^{206}\text{Pb}/^{238}\text{U}$ age of 305 ± 1.3 Ma (MSWD = 1.14) (Fig. 5d).

6.2 Geochemical and isotopic characteristics

The results for bulk-rock analysis are given in Table 3. The rocks of the DF vary significantly in composition, including basalt, trachybasalt, basaltic trachybasalt, basaltic andesite, trachy-andesite, dacite and rhyolite. The DF volcanic rocks plot in the calc-alkaline field in $\text{FeO}^{\text{T}}\text{-MgO}$

Table 2 Petrography of studied samples

Sample	Rock type	Petrographic description
CGNE-3	Volcanic rock	Fresh; glass shards (>40 %), crystal clasts of plagioclase and andesitic clasts (~15 %) and very fine-grained volcanic ash (~45 %)
CGNE-15	Volcanic rock	Porphyritic and fresh; ~15 % phenocrysts and 85 % groundmass; Phenocrysts: plagioclase (~10 %) and amphibole (~5 %)
ZB-3	Volcanic rock	Porphyritic and fresh; ~12 % phenocrysts and 83 % groundmass and ~5 % clasts
ZB-8	Volcanic rock	Porphyritic and fresh; ~10 % phenocrysts and 88 % groundmass and ~2 % clasts
ZB-17	Volcanic rock	Porphyritic and fresh; ~17 % phenocrysts and 83 % groundmass; phenocrysts: plagioclase (~9 %) and amphibole (~8 %)
ZB-19	Volcanic rock	Fresh; glass shards (>35 %), crystal clasts of plagioclase, amphibole, andesitic clasts (~15 %) and very fine-grained volcanic ashes (~50 %)
CGNE-6	Massive ore	Massive structure, >90 % magnetite, ~8 % pyrite and ~2 % gangue minerals
CGNE-14	Massive ore	Massive structure, >90 % magnetite, ~10 % pyrite
CGNE06-5.9	Granodiorite	Fresh; feldspar (~14 %), plagioclase (~30 %), quartz (~30 %), biotite (~5 %) and amphibole (~21 %)
CGNE06-546	Granodiorite	Fresh; feldspar (~8 %), plagioclase (~23 %), quartz (~35 %), biotite (~10 %) and amphibole (~24 %)

space (Fig. 6a). The chondrite-normalized rare earth element (REE) patterns of andesitic samples are characterized by light REE-enrichment, relatively flat heavy REEs and a subtle negative Eu anomaly (Fig. 6f). Sr and Nd isotopic compositions of volcanic rocks are given in Table 4. Andesitic rocks have high $^{87}\text{Sr}/^{86}\text{Sr}_{(i)}$ values varying from 0.7058 to 0.7117, and their $\varepsilon_{\text{Nd}}(t)$ values range from -3.51 to 1.67 (Table 4). Basalt in the Chagangnuoer deposit gives $\varepsilon_{\text{Nd}}(t) > 0$, which indicate that their source is depleted mantle [30]. The TiO_2 and P_2O_5 abundances in the massive ores ($\text{FeO}^{\text{T}} > 85$ wt %) are very low, varying from 0.022 to 0.117 wt %, from 0.045 to 0.163 wt %, respectively (Table 3).

The 305 Ma granodiorite samples have SiO_2 contents varying from 62.39 to 71.70 wt % and plot in calc-alkaline field of $\text{FeO}^{\text{T}}\text{-MgO}$ space (Fig. 6a), and their FeO^{T} contents decrease with increasing SiO_2 (Fig. 6b). They have A/CNK [molar $\text{Al}_2\text{O}_3/(\text{CaO} + \text{Na}_2\text{O} + \text{K}_2\text{O})$] of 0.86–1.02 and $\text{K}_2\text{O}/\text{Na}_2\text{O}$ ratios between 0.8 and 2.6. The chondrite-normalized REE pattern is characterized by enrichment in LREEs, flat HREEs and a negative Eu anomaly (0.47–0.61) (Fig. 6d). Furthermore, on primitive mantle-normalized spider diagrams, the samples show enrichments in LILEs with distinct negative Nb, Ta and Ti anomalies (Fig. 6c).

7 Discussion

7.1 Granitoids in ore district

The tectonic setting for the Later Carboniferous country rocks in the AMB is still controversial, including intra-

continental rift [50, 51], post-collisional mantle plumes [52, 53] and active continental margin [28, 30]. Recently, U–Pb ages of 321 and 302 Ma [28, 30] have been obtained for the DF rhyolite from the Chagangnuoer iron deposit, and the geochemical characteristics of these rocks indicate that they formed in an active continental margin setting. Furthermore, all of the DF volcanic rocks in the eastern AMB display calc-alkaline series with arc-affinity, including 300 Ma dacite and 329 Ma andesite in the Zhibo deposit [14, 28], 301 Ma dacite and 304 Ma rhyolite in the Beizhan deposit [32] and 316 Ma dacite in the Dundee deposit [7]. The geochemical characteristics of the granitoids in this district may give some hints regarding the tectonic setting of the region in the Late Carboniferous. The composition of the granitoids in the eastern part of AMB, including the 305 Ma granodiorite in the Chagangnuoer deposit and 319 Ma diorite and 304 Ma granite intrusions in the Zhibo deposit, also indicates an arc-affinity, i.e., enrichment of LILE and LREE with distinct depletion of Nb, Ta, Ti and HREE. Thus, these age data and their geochemical characteristics demonstrate that the DF and granitoids in the northeastern AMB are products of multiple magmatism of 300–320 Ma in a subduction-related environment.

Hong et al. [13] reported a mineralization-associated garnet Sm–Nd isochron age of 317 Ma for the Chagangnuoer deposit, which differs from the zircon U–Pb age of granitoids (305, 250 Ma). This indicates that the granitoids have no contribution to the skarn development. Moreover, the DF volcanic rocks (300–320 Ma) and granitoids (305 Ma) in the Chagangnuoer deposit display calc-alkaline characteristics (Fig. 6a), which indicate that their evolved melt via fractional crystallization does not

Table 3 Major and trace element abundances of andesitic rocks, granodiorite and ores

Sample	Andesitic rocks						Granodiorite						Ores			
	CGNE-3	CGNE-15	ZB-3	ZB-8	ZB-17	ZB-19	CGNE12-35	ZK06-5-9	ZK06-209	ZK06-546	ZK06-830	CGNE-6	CGNE-14	CGNE-16		
SiO ₂	55.19	55.90	52.33	52.54	53.19	54.67	66.50	62.39	64.48	66.46	71.70	1.349	5.044	6.552		
TO ₂	0.706	0.909	0.701	0.780	0.714	0.861	0.738	0.829	0.748	0.821	0.420	0.022	0.117	0.042		
Al ₂ O ₃	10.32	14.18	17.10	14.76	11.86	18.61	13.40	15.02	13.43	13.60	12.10	2.012	0.727	1.081		
Fe ₃ O ₄ ^T	11.31	5.938	5.007	11.96	8.967	7.745	5.452	8.022	6.682	5.823	3.942	92.96	91.70	87.24		
MnO	0.300	0.223	0.189	0.095	0.322	0.157	0.315	0.109	0.151	0.124	0.062	0.146	0.113	0.107		
MgO	9.049	5.730	6.029	5.237	10.18	4.589	2.676	3.325	3.273	2.502	0.820	1.690	1.384	1.134		
CaO	4.593	5.806	12.36	8.088	8.856	3.262	2.705	3.918	3.977	3.291	1.723	2.953	1.792	2.010		
Na ₂ O	2.713	2.000	3.347	4.321	3.007	6.019	2.208	3.011	2.801	2.931	2.339	0.105	0.045	0.037		
K ₂ O	2.032	7.324	0.883	0.665	0.661	1.217	4.219	2.401	3.456	3.349	6.026	0.056	0.097	0.055		
P ₂ O ₅	0.208	0.131	0.104	0.089	0.117	0.132	0.140	0.186	0.146	0.156	0.056	0.045	0.163	0.145		
LOI	2.527	1.101	1.390	0.811	1.344	1.858	1.376	0.495	0.478	0.659	0.615	-1.020	-1.032	1.742		
Total	98.96	99.24	99.43	99.34	99.22	99.12	99.73	99.71	99.63	99.71	99.80	100.3	100.1	100.1		
Li	24.82	7.352	9.664	2.242	9.986	19.84	21.74	27.86	15.76	20.60	11.20					
P	872.4	514.0	423.0	345.2	465.8	528.6	1,045	1,202	1,075	1,167	475.0					
K	16,906	56,340	6,982	5,234	5,340	9,866	53,360	28,260	42,320	42,320	77,780					
Sc	17.53	32.54	31.66	36.17	24.99	20.44	27.62	27.70	27.44	26.06	9.784					
Ti	4,826	5,790	4,646	5,070	4,682	5,522	7,052	7,150	6,792	7,650	3,728					
V	153.8	162.2	250.0	369.0	182.1	219.4	196.5	241.6	232.2	188.9	60.52					
Cr	839.6	146.3	29.70	14.11	661.6	15.61	58.40	61.84	64.96	57.80	19.02					
Mn	2,350	1,650	1,392	677.0	2,357	1,144	3,538	1,082	1,632	1,321	569.6					
Co	37.72	7.664	7.346	10.16	17.49	5.948	15.47	21.86	23.00	19.79	25.42					
Ni	320.2	15.20	12.28	29.46	128.2	13.80	16.52	30.66	30.72	25.08	13.90					
Cu	12.65	4.213	5.067	3.133	2.931	2.845	21.70	2.478	7.448	34.14	3.722					
Zn	263.4	75.06	44.90	36.12	97.71	80.98	184.0	70.00	71.12	97.40	58.16					
Ga	17.86	12.57	16.92	17.33	15.02	16.45	18.70	19.50	18.47	16.64	13.97					
Rb	62.22	230.6	58.04	31.96	26.69	109.5	230.6	132.3	162.0	144.1	221.4					
Sr	174.5	224.8	319.6	299.6	219.6	254.8	281.4	221.6	249.6	365.2	126.3					
Y	10.96	19.44	23.14	20.02	26.14	15.78	36.56	18.54	21.11	22.59	20.94					
Zr	92.80	130.7	47.68	43.72	119.5	65.34	269.4	190.8	188.4	278.0	263.0					
Nb	2.111	4.441	2.824	2.117	4.493	3.211	12.91	9.558	7.982	10.88	11.68					
Cs	1.448	0.887	1.140	0.340	0.418	2.756	0.807	2.114	1.116	1.319	0.842					
Ba	708.0	1980	226.6	115.8	144.2	114.2	925.6	272.6	529.2	497.4	486.6					
La	5.676	34.10	12.33	29.50	4.826	14.10	12.33	12.13	13.93	13.77	17.43	16.03	15.05	8.496		
Ce	15.95	69.56	18.87	45.62	20.91	25.42	28.36	27.24	30.08	32.26	38.12	19.73	23.48	13.87		

Table 3 continued

Sample	Andesitic rocks							Granodiorite							Ores			
	CGNE-3	CGNE-15	ZB-3	ZB-8	ZB-17	ZB-19	CGNE12-35	ZK06-5.9	ZK06-209	ZK06-546	ZK06-830	CGNE-6	CGNE-14	CGNE-16				
Pr	2.400	7.464	1.942	4.448	3.664	3.036	3.840	3.386	3.672	4.100	4.408	1.389	2.278	1.447				
Nd	11.87	27.00	8.128	17.01	18.79	13.21	16.72	13.47	14.46	16.48	15.77	3.692	7.860	5.440				
Sm	2.882	4.474	2.554	3.456	5.045	2.942	4.818	3.250	3.348	3.832	3.286	0.330	1.213	1.035				
Eu	0.798	1.500	1.010	1.278	1.152	0.859	1.028	0.691	0.699	0.808	0.499	0.055	0.223	0.177				
Gd	2.742	4.334	3.606	3.892	5.231	3.144	5.528	3.382	3.530	3.960	3.184	0.332	1.240	1.155				
Tb	0.398	0.621	0.644	0.599	0.816	0.472	0.930	0.524	0.552	0.611	0.512	0.035	0.153	0.163				
Dy	2.326	3.790	4.336	3.818	5.061	2.984	6.002	3.190	3.420	3.746	3.230	0.191	0.873	0.989				
Ho	0.450	0.778	0.930	0.808	1.051	0.627	1.277	0.652	0.723	0.795	0.687	0.046	0.185	0.215				
Er	1.273	2.356	2.788	2.420	3.144	1.885	3.724	1.834	2.090	2.286	2.082	0.164	0.576	0.681				
Tm	0.174	0.338	0.396	0.343	0.451	0.272	0.545	0.260	0.306	0.337	0.313	0.029	0.085	0.104				
Yb	1.157	2.342	2.626	2.348	3.093	1.886	3.562	1.696	2.026	2.208	2.084	0.246	0.656	0.821				
Lu	0.173	0.369	0.383	0.358	0.460	0.286	0.505	0.254	0.300	0.330	0.305	0.059	0.129	0.156				
Hf	2.286	3.175	1.179	1.112	2.730	1.548	6.487	4.692	4.601	6.624	6.679							
Ta	0.137	0.305	0.207	0.123	0.298	0.197	0.885	0.626	0.487	0.659	0.903							
Pb	4.194	2.860	5.256	2.174	2.571	1.354	43.70	4.050	4.392	3.700	5.390							
Th	0.828	6.865	0.755	0.774	8.514	1.417	12.03	8.384	7.386	11.52	19.46							
U	0.322	7.022	4.030	2.800	7.982	1.820	1.842	1.623	2.322	3.236	6.050							

Table 4 Sr–Nd isotopic compositions of the representative andesitic volcanic samples from Chagangnuoer deposits. CGNE-3 and CGNE-15 are from Chagangnuoer deposit

Sample	Lithology	Rb (ppm)	$^{87}\text{Sr}/^{86}\text{Sr}$	$^{87}\text{Sr}/^{86}\text{Sr}_{(i)}$	$\pm 2\sigma$	Nd (ppm)	$^{143}\text{Nd}/^{144}\text{Nd}$	$\pm 2\sigma$	$\varepsilon_{\text{Nd}}(t)$
CGNE-3	Andesitic tuff	62.22	0.70877	0.70679	6×10^{-6}	11.87	0.512900	7×10^{-6}	1.67
CGNE-15	Andesite	230.6	0.71736	0.71167	5×10^{-6}	27.00	0.512649	5×10^{-6}	0.26
ZB-3	Andesitic rock	58.04	0.70718	0.70583	5×10^{-6}	8.128	0.512800	5×10^{-6}	−1.09
ZB-8	Andesitic rock	31.96	0.70643	0.70617	5×10^{-6}	17.01	0.512666	6×10^{-6}	−3.51
ZB-17	Andesitic rock	26.69	0.70667	0.70599	5×10^{-6}	18.79	0.512763	5×10^{-6}	−2.15
ZB-19	Andesitic rock	109.5	0.71022	0.70783	6×10^{-6}	13.20	0.512624	4×10^{-6}	−2.81

ZB-3, ZB-8, ZB-17 and ZB-19 are from Zhibo deposit

$$^{87}\text{Sr}/^{86}\text{Sr}_{(\text{present})} = ^{87}\text{Sr}/^{86}\text{Sr}_{(i)} + ^{87}\text{Rb}/^{86}\text{Sr}_{(\text{present})} \times (e^{\lambda t} - 1), \text{ where } \lambda = 1.42 \times 10^{-11}, t = 300 \text{ Ma}, ^{143}\text{Nd}/^{144}\text{Nd}_{(\text{present})} = ^{143}\text{Nd}/^{144}\text{Nd}_{(i)} + ^{147}\text{Sm}/^{144}\text{Nd}_{(\text{present})} \times (e^{\lambda t} - 1), \text{ where } \lambda = 6.54 \times 10^{-12}, t = 300 \text{ Ma}$$

$$\varepsilon_{\text{Nd}}(t) = \left[\frac{^{143}\text{Nd}/^{144}\text{Nd}_{(\text{rock}(t))}}{^{143}\text{Nd}/^{144}\text{Nd}_{\text{CHUR}(t)}} - 1 \right] \times 10,000, \text{ where, } ^{143}\text{Nd}/^{144}\text{Nd}_{\text{CHUR}(\text{present})} = ^{143}\text{Nd}/^{144}\text{Nd}_{\text{CHUR}(t)} + ^{147}\text{Sm}/^{144}\text{Nd}_{\text{CHUR}(\text{present})} \times (e^{\lambda t} - 1), ^{143}\text{Nd}/^{144}\text{Nd}_{\text{CHUR}(\text{present})} = 0.512638, ^{147}\text{Sm}/^{144}\text{Nd}_{\text{CHUR}(\text{present})} = 0.1967, \lambda_{\text{sm}} = 6.54 \times 10^{-12}$$

have Fe-rich characteristics. Therefore, the models of iron-rich fluid/melt derived from evolved magmas [54] cannot be applied to explain the ore genesis of the Chagangnuoer deposit.

7.2 The petrogenesis of andesitic rocks

As discussed above, the DF volcanism was genetically associated with a subduction-zone environment. It is likely that the basalts of DF in the Chagangnuoer deposit were derived from depleted mantle wedge [30]. However, the petrogenesis of ore-bearing andesitic rocks remains poorly understood. In order to evaluate the potential magma source for the andesitic rocks, we need to consider processes that can effectively explain the composition of these rocks, especially the trace element characteristics and isotopic signatures. The generation of intermediate arc magmas is widely attributed to three main processes: differentiation of primary mafic magmas by crystallization within the crust or uppermost mantle [55, 56], partial melting of older crustal rocks [57, 58] and basaltic magmas were contaminated by crustal felsic materials with or without fractional crystallization [59, 60].

The andesitic rocks have low $\varepsilon_{\text{Nd}}(320 \text{ Ma})$ (−3.51 to 1.67, Fig. 7b) than basalt (5.7–7.3) [30] from the DF in Chagangnuoer iron deposit. Therefore, fractional crystallization of basaltic magmas cannot account for the isotopic compositions of andesitic volcanic rocks in the Chagangnuoer deposit. Moreover, the main constituent of the DF is andesitic rather than basaltic rocks. The volumetrically significant andesitic rocks require partial melting of basaltic rocks as has been well-established (see [61] for a review).

The old mafic lower crust of the AMB is represented by the Tianshan Proterozoic metamorphic basement, whose

$\varepsilon_{\text{Nd}}(320 \text{ Ma})$ range from −8 to −4 [62, 63]. Such low ε_{Nd} precludes the possibility that the andesitic volcanic rocks ($\varepsilon_{\text{Nd}}(320 \text{ Ma}) = -3.51$ to 1.67) were derived from such old mafic lower crust.

The DF andesitic rocks may thus have been generated from basaltic magmas via crustal assimilation, i.e., a mixing process. In the andesitic rocks of the DF, Th/Ta ratios increase with increasing Zr/Nb and SiO_2 (Fig. 7a, c). These geochemical features tend to suggest that the parental magma of these andesitic rocks may have been contaminated by crustal materials, which are further supported by the positive correlation between SiO_2 and $^{87}\text{Sr}/^{86}\text{Sr}_{(i)}$ for the andesitic rocks (Fig. 7d). Since the basaltic rocks in DF are derived from depleted mantle [30], we select DM and enriched lower crust as end-member components to evaluate the isotopic signatures of the DF andesitic volcanic rocks. As shown in Fig. 7b, mixing of depleted mantle and enriched crust can well explain the isotopic characteristics of andesitic rocks in DF.

The foregoing discussion and reasoning suggest that the petrogenesis of the DF andesitic rocks may have resulted from mantle-derived basaltic magma with significant continental crustal assimilation or mixing, which better explain the chemical and isotopic data than other suggestions discussed above.

7.3 The origin of iron mineralization

The Chagangnuoer deposit is a typical SVIO deposit in the western Tianshan, China [25]. The origin of the Chagangnuoer iron deposit, like similar deposits elsewhere such as Yamansu, Abagong, Anzas and Tuomuerte iron deposits, is in debate and has been interpreted differently: (1) magmatic origin [64, 65]; (2) exhalative-

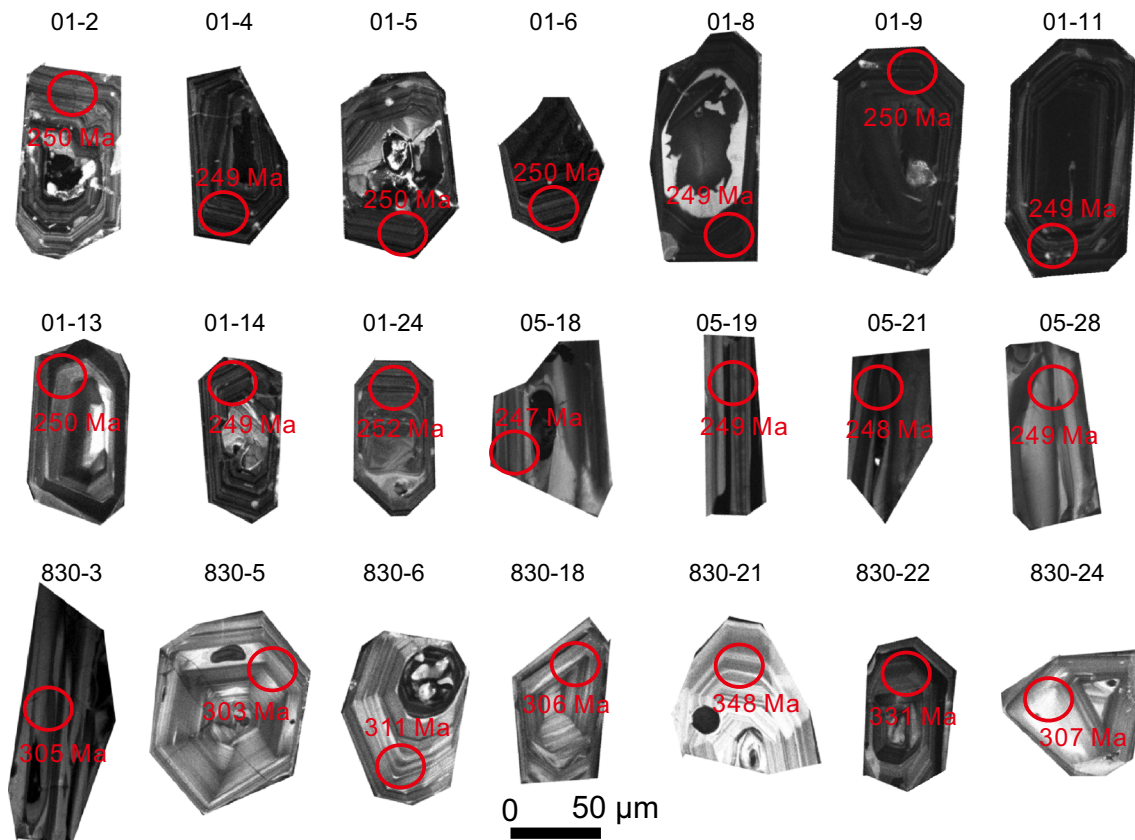


Fig. 4 Representative CL images from granitoids in the Chagangnuoer deposit. Sample CGNE12-01 is abbreviated to 01, CGNE12-05 to 05 and ZK06-830 to 830

synsedimentary [66]; and (3) hydrothermal replacement (skarnization) deposit [11, 12, 16]. Although magmatic origin model is used to explain the genesis of some SVIO deposits with signatures of magmatic origin, such as high proportion of apatite in the magnetite ores (e.g., Abagong in Altay, [65, 67]), but how the ore-bearing melt formed is still unclear [25, 68]. Moreover, some of the SVIO deposits have very low contents of P, Ti and display no P, Ti correlation with FeO^T in massive iron samples (Fig. 8), which argue against the magmatic origin as a result of oxide melt immiscibility (and fractional crystallization) from the silicate magmas [54, 69]. If exhalative-synsedimentary model is applicable, considering the submarine volcanic environment, the deposit should be accompanied by other facies of chemical exhalite, such as pyritic chert, jasper and Fe-Mn oxide deposits [68]. However, these have not been recognized in the Chagangnuoer deposit and elsewhere, such as Yamansu deposit [8]. We suggest that the metallogensis of the Chagangnuoer deposit should be genetically associated with skarn formation because: (1) the skarn is pervasive around ore bodies and the paragenetic textures between skarn minerals and magnetite are conspicuous under microscope (Figs. 1c, 2, 3b, c, f, i); (2)

the mineral assemblages of grossular garnet, diopsidic-hedenbergitic pyroxene and epidote are consistent with typical skarn iron deposits [4, 16]; and (3) the timing of the skarn formation (316 ± 6.7 Ma) is essentially the same within error as the iron mineralization [13–15].

Like Chagangnuoer iron deposit, skarn minerals (e.g., diopside and garnet) are extensively developed in some SVIO deposits, such as Dundee and Yamansu iron deposits [7, 8]. The common feature of these deposits is the fact that the host rocks all contain carbonate rocks [25]. However, these iron skarn deposits occur within volcanic rocks and are unrelated to the intrusive rocks in time and space. Therefore, reaction modeling cannot be applied to such volcanic-hosted skarn iron deposits. Two competing models have been proposed to explain the origin(s) of these skarns and associated iron mineralization: (1) metasomatism by fluids related to the exhalation of coeval submarine volcanism or deep intrusions [8–10, 16, 70]; and (2) “deep skarn environment” origin [20–24]. The iron source in the first models remains controversial, such as leaching from host rocks by fluids [8] or sequestering from magmas by fluids [29]. Moreover, what causes iron precipitation to form deposits in volcanic rocks remains an enigma. The “deep skarn

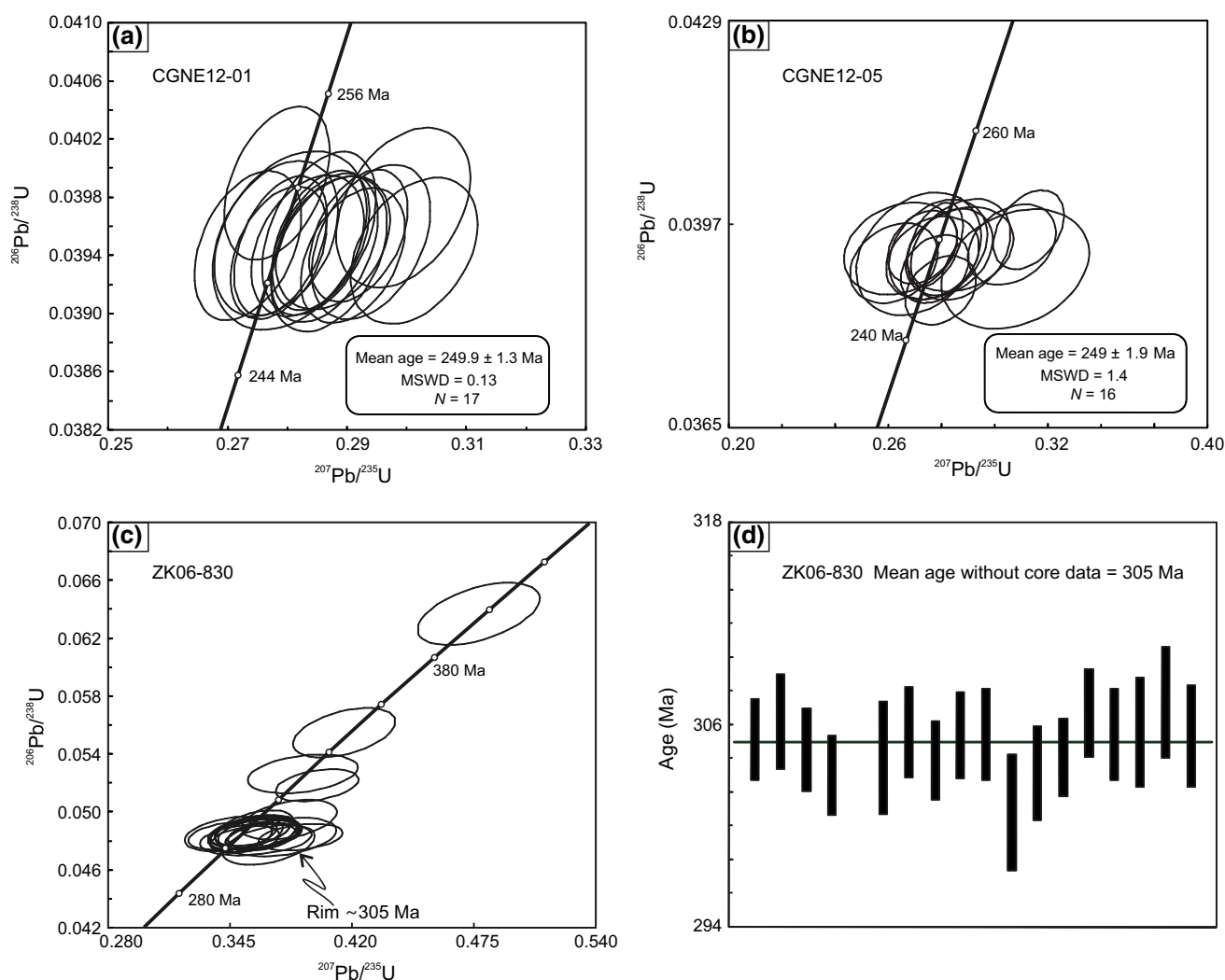


Fig. 5 a, b and c are Laser ablation ICP-MS U–Pb zircon concordia diagrams of granitoids in the Chagangnuoer deposit. d shows weighted average age for ZK06-830 without core data

environment” model suggests that deep magmas assimilate limestone and undergo subsequently immiscible separation of iron-enriched ore melts. However, the cause(s) that led to iron-enriched ore melt immiscibility is poorly understood. Based on observations on the Chagangnuoer deposit, we envisage a new ore-forming process as follows for volcanic-hosted skarn iron deposits.

As discussed above, skarn is important to metallogenesis of the Chagangnuoer deposit. The skarn forming and magmatism of the volcanic rocks are coeval. Ore-bearing andesitic rocks of DF have been generated from basaltic magmas via crustal contamination. Carbonate rocks of Proterozoic, Silurian, Devonian and Carboniferous are abundant [15]. For example, within the DF alone, the limestone is about 300 m thick [14]. Therefore, during ascent through the crust, the basaltic magma not only assimilate/contaminate the silicate rocks, but also reacts

with the limestone. High-temperature basaltic magma will lead limestone to melt directly under low $\text{CO}_2/\text{H}_2\text{O}$ environment [71]. The generated carbonate melts can react with basaltic magmas to form skarn minerals. Since in the reaction of basaltic magmas with carbonates, skarn products have consumed Si–O thought to be bound to Fe during evolution of slowly cooling basaltic magmas. As shown in Fig. 9, the residual components become FeO^{T} -rich after reaction. The “excess” iron component (relative to Si, Ca and Mg consumed) combine with CO_3^{2-} to form Fe(II) carbonate complex (e.g., $\text{FeCO}_3[\text{aq}]$, FeCO_3^{2-} , [72]). This explains how iron becomes separated from silicate melts and concentrated in the infiltrating fluids.

Percolation and migration of the FeCO_3 -fluids toward surface will lead to magnetite precipitation through the following reaction, favored by decreasing pressure and temperature:

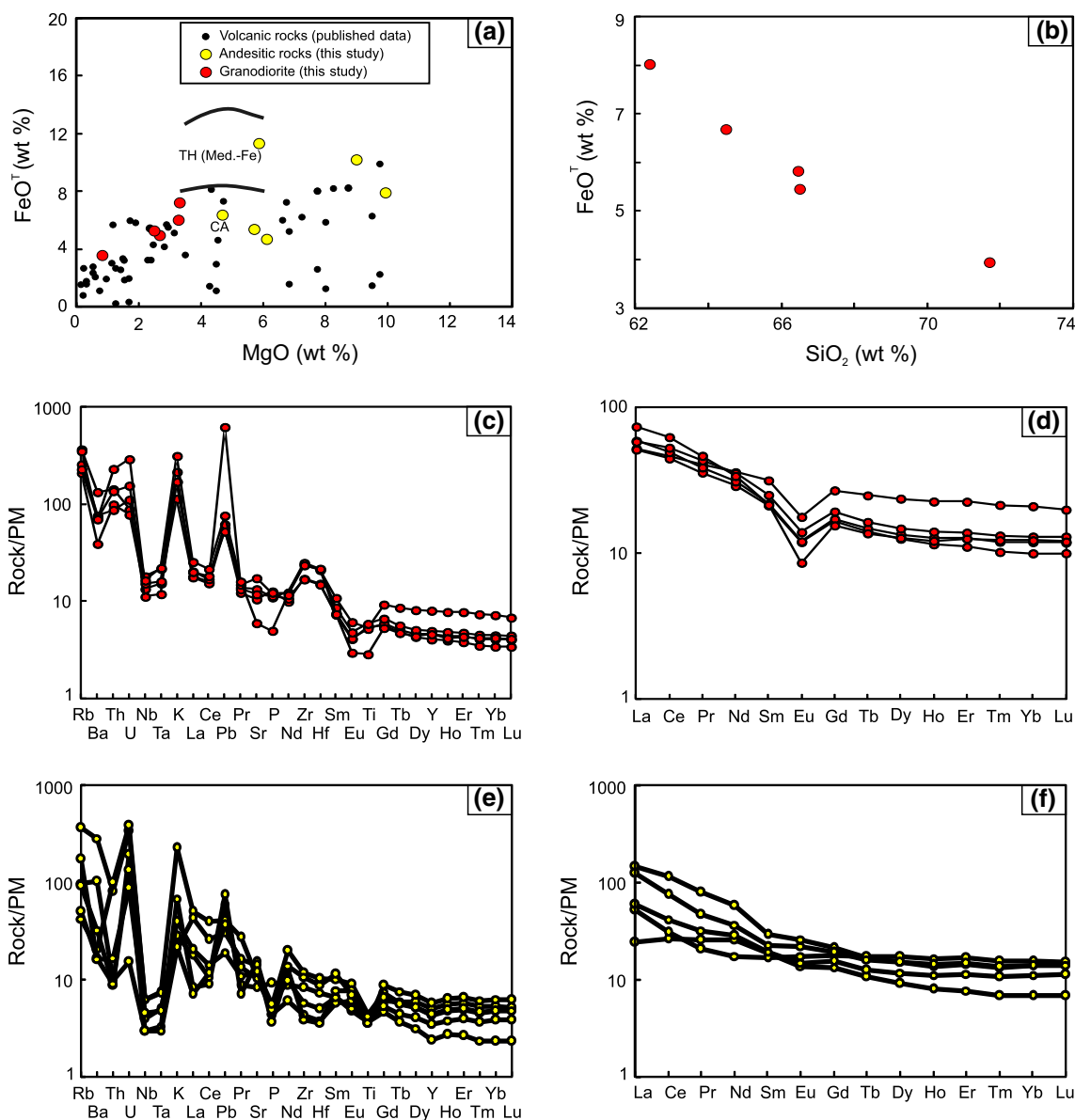


Fig. 6 **a** FeO^T–MgO diagram of volcanic rocks and granitoids (after Pearce et al. [48]); **b** FeO^T–SiO₂ plots of 305 Ma granitoid. Primitive mantle-normalized spidergrams of the granitoid (c) and andesitic rocks (e), normalization values after Sun et al. [49]. Chondrite-normalized REE patterns of the granitoid (d) and andesitic rocks (f), normalization values after Sun et al. [49]. Yellow circles represent andesitic rocks from this study, and red circles represent granitoids (G) from this study. Blank circles represent volcanic rocks of DF from triangles represent volcanic rocks of DF [10, 28, 30]



8 Conclusions

- (1) The Chaganguoer deposit is a typical submarine volcanic-hosted skarn iron deposit, where orebodies occur in andesitic volcanic rocks with well-developed
- (2) LA-ICP-MS U–Pb zircon ages of 250 and 305 Ma are obtained for granite and granodiorite in the

skarns around orebodies. The ore-bearing andesitic rocks have high ⁸⁷Sr/⁸⁶Sr_(i) values varying from 0.7058 to 0.7117, and their ε_{Nd}(320 Ma) values range from –3.51 to 1.67. They probably formed through mixing of basaltic melts and the induced crustal melts. The DF volcanic rocks display calc-alkaline characteristics.

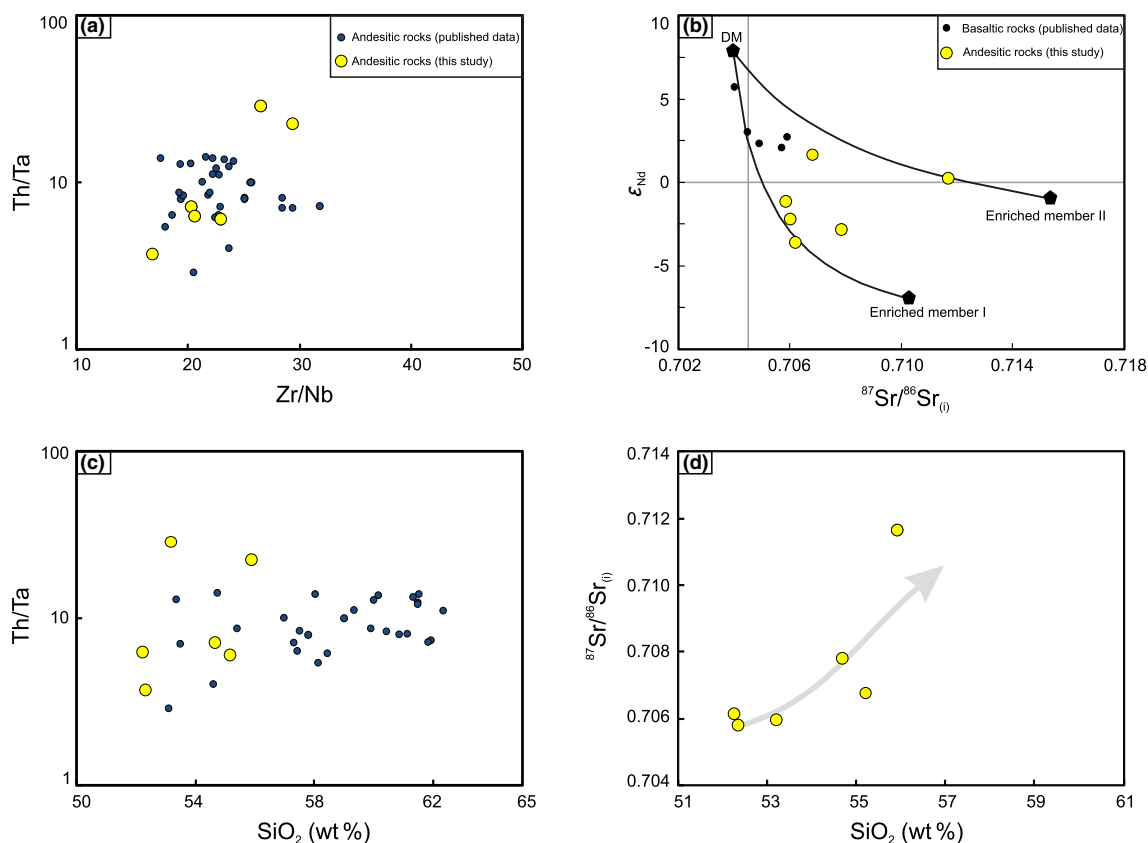


Fig. 7 Diagrams of Zr/Nb vs. Th/Ta (a), $^{87}\text{Sr}/^{86}\text{Sr}_{(i)}$ vs. $\epsilon_{\text{Nd}}(t)$ (b), Th/Ta vs. SiO_2 (c) and $^{87}\text{Sr}/^{86}\text{Sr}_{(i)}$ vs. SiO_2 (d) for andesitic volcanic rocks of DF. Yellow circles are from this study. The blue and black circles are published data, which are from Feng et al. [15], Zhu et al. [41], Wang et al. [30] and Jiang et al. [28]. DM represent depleted mantle with $^{87}\text{Sr}/^{86}\text{Sr}_{(i)} = 0.703946$ and $\epsilon_{\text{Nd}}(t) = 7.86$. Both of enriched member I and II are from Chen et al. [62] and Hu et al. [63], I with $^{87}\text{Sr}/^{86}\text{Sr}_{(i)} = 0.710214$ and $\epsilon_{\text{Nd}}(300 \text{ Ma}) = -6.92$ and II with $^{87}\text{Sr}/^{86}\text{Sr}_{(i)} = 0.715214$ and $\epsilon_{\text{Nd}}(t) = -0.86$

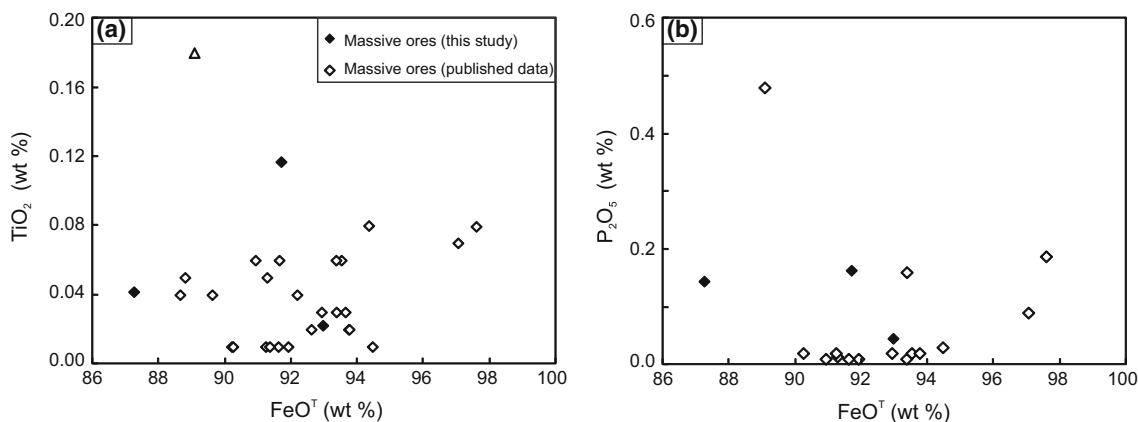


Fig. 8 Plots of TiO_2 vs. FeO^{T} (a) and Plots of P_2O_5 vs. FeO^{T} (b) for massive ores and magnetite composition. Published data are from Hong et al. [4]

Chaganuoe deposit, which are significantly younger than the skarn formation, thus the granitoids have no contribution to skarn and associated iron mineralization.

(3) This paper proposes a new model for the genesis of volcanic-hosted skarn Fe deposits (Fig. 10). This model emphasizes that (i) iron separates from silicate magmas in the form of Fe(I) carbonate complex; and

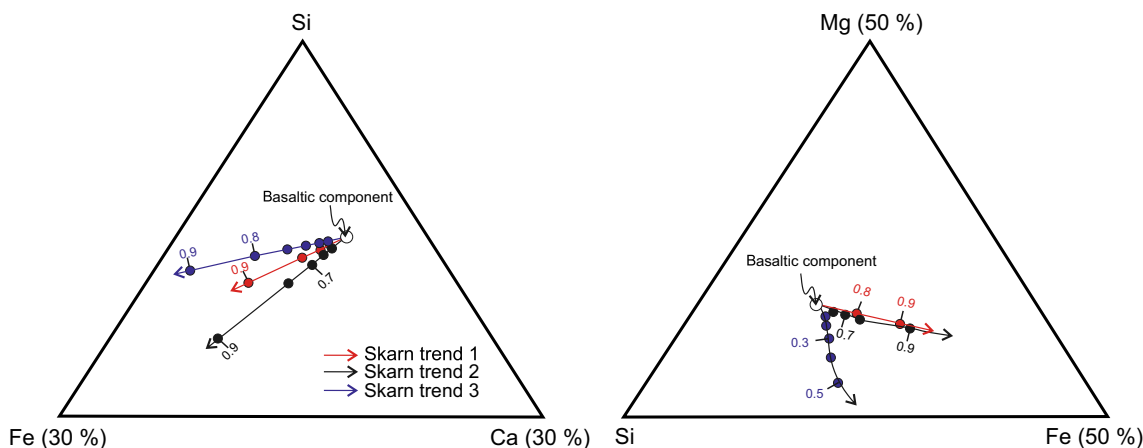


Fig. 9 Ternary plots show that basaltic magma component changes before and after representative skarn forming in our research area. All element abundance has been turned to mole percent. Vectors show the compositional changes driven by skarns formed and the minerals proportions (by weight) in the skarn trend 1, 2 and 3 are $Ep_{0.1}Di_{0.4}Gt_{0.4}$, $Di_{0.5}Gt_{0.5}$ and $Di_{0.15}Gt_{0.85}$, respectively. Tick marks on the curves show the extracted weight fraction of skarns. The garnet data are from Feng et al. [15]; the clinopyroxene and epidote data are from Hong et al. [4] and Jiang et al. [28]

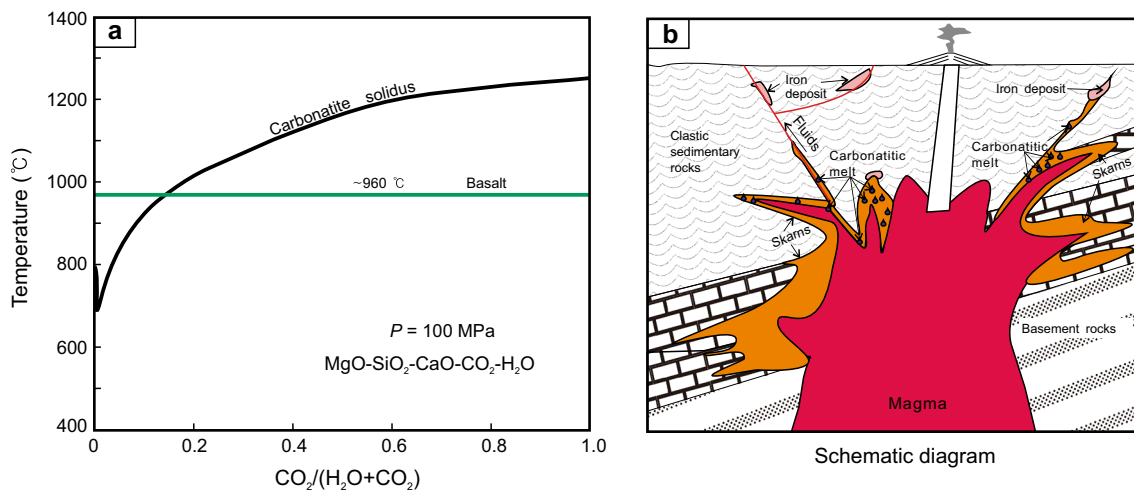


Fig. 10 Temperature vs. CO_2/H_2O show the carbonatite solidus (a modified after Wenzel et al. [71]), the temperature of basaltic temperature under 100 MPa are from Stem et al. [73]; Schematic diagram of hypothetical relationships between iron deposits and magma and limestone (b modified after Lentz et al. [74])

(ii) this complex results from interaction between limestone-generated carbonate melts and basaltic components. When the fluids containing Fe(II) carbonates complex move toward the surface, magnetite precipitate as a result of decreasing temperature and pressure.

(4) While this conceptual model is largely based on observations on the Changanuoer deposit, it may have general significance for skarn-type Fe deposits associated with marine volcanic rock sequences,

recognized in many orogenic belts, including the giant deposits in the Lhasa Terrane. We also emphasize that our genetic model warrants further testing and improvement.

Acknowledgments The authors are grateful to the Third and Eleventh Geological Survey Institute for logistical support during field work at the Changanuoer orefield, as well as Xi'an Centre of Geological Survey, CGS. This work was supported by two geological survey projects of China Geological Survey Departments and Offices (1212011121092, 1212011220928).

Conflict of interest The authors declare that they have no conflict of interest.

References

- Belevtsev YN (1982) Volcanogenic-sedimentary origin of magnetite ores of the Urals. *Int Geol Rev* 24:1405–1416
- Mao JW, Goldfar RJ, Wang YT et al (2005) Late Paleozoic base and precious metal deposits, East Tianshan, Xinjiang, China: characteristics and geodynamic setting. *Episode* 28:23–36
- Hong W, Zhang ZH, Jiang ZS et al (2012) Magnetite and garnet trace element characteristics from the Chagangnuoer iron deposit in the western Tianshan Mountains, Xinjiang, NW China: constrain for ore genesis. *Acta Petrol Sin* 28:2089–2102 (in Chinese)
- Hong W, Zhang ZH, Zhao J et al (2012) Mineralogy of Chagangnuoer iron deposits in Western Tianshan Mountains, Xinjiang, China. *Acta Petrol Miner* 31:191–211 (in Chinese)
- Amina Gong XP, Xu XJ (2012) The ore geology and ore-bearing rocks alteration in Beizhan deposit. *West Ore Prospect* 3:171–173 (in Chinese)
- Amina Gong XP, Alina et al (2013) The geology, geochemistry of Dahalajunshan Formation volcanic rocks in Beizhan deposit, western Tianshan. *Xinjiang Geol* 32:129–135 (in Chinese)
- Duan SG, Zhang ZH, Jiang ZSH et al (2014) Geology, geochemistry, and geochronology of the Dundee iron–zinc ore deposit in western Tianshan, China. *Ore Geol Rev* 57:441–461
- Hou T, Zhang ZC, Santosh M et al (2014) Geochronology and geochemistry of submarine volcanic rocks in the Yamasu iron deposit, Eastern Tianshan Mountains, NW China: constraints on the metallogenesis. *Ore Geol Rev* 56:487–502
- Li Q, Zhang ZX, Geng XX et al (2014) Geology and geochemistry of the Qiaoxiahala Fe–Cu–Au deposit, Junggar region, northwest China. *Ore Geol Rev* 57:462–481
- Jiang ZS, Zhang ZH, Wang ZH et al (2014) Geology, geochemistry, and geochronology of the Zhibo iron deposit in the western Tianshan, NW China: constraints on metallogenesis and tectonic setting. *Ore Geol Rev* 57:406–424
- Battles DA, Barton MD (1995) Arc-related sodic hydrothermal alteration in the western US. *Geology* 23:913–916
- Franchini MB, DeBarrio RE, Pons MJ et al (2007) Fe skarn, iron oxide Cu–Au, and Manto Cu–(Ag) Deposits in the Andes Cordillera of southwest Mendoza province (34°–36°S), Argentina. *Explor Min Geol* 16:233–265
- Hong W, Zhang ZH, Li HQ et al (2012) Metallogenic epoch of Chagangnuoer iron deposit in western Tianshan Mountains, Xinjiang: information from garnet Sm–Nd isochronal age. *Miner Deposita* 31:1067–1074
- Zhang X, Tian JQ (2012) Geochronology and geochemistry of granitoid rocks from the Zhibo syngenetic volcanogenic iron ore deposit in the Western Tianshan Mountains (NW-China): constraints on the age of mineralization and tectonic setting. *Gondwana Res* 57:585–596
- Feng JX, Shi FP, Wang BY et al (2010) Volcanic iron ore deposits in Awulale metallogenic belt in Western Tianshan. Geological Publishing House, Beijing, pp 1–92 (in Chinese)
- Meinert LD, Dippl GM, Nicolescu S (2005) World Skarn deposits. *Econ Geol* 100:299–366
- Fulignati P, Marianelli P, Santacrose R et al (2004) Probing the Vesuvius magma chamber-host rock interface through xenoliths. *Geol Mag* 141:417–428
- Gilg HA, Lima A, Somma R et al (2001) Isotope geochemistry and fluid inclusion study of skarns from Vesuvius: Special issue on Mt. Somma-Vesuvius and volcanism of the Campanian Plain. *Miner Petrol* 73:145–176
- Matthews SJ, Marquillas RA, Kemp AJ et al (1996) Active skarn formation beneath Lascar Volcano, northern Chile: a petrographic and geochemical study of xenoliths in eruption products. *J Metamorph Geol* 14:509–530
- Wu YC (1992) The discussion of skarn magma: a new kinds of skarn rocks. *Geol Anhui* 2:12–26 (in Chinese)
- Wu YC, Shao GQ, Wu L (1996) The skarn magma and associated deposits. *Geol Anhui* 6:30–39 (in Chinese)
- Wu YC, Chang YF (1998) Some ideal about magmatic skarn. *Earth Sci Front* 5:291–301 (in Chinese)
- Chen Y, Zhang ZC (2012) Study on source, transportation and the enrichment mechanism of iron skarn deposit. *Miner Rock Anal* 31:889–897 (in Chinese)
- Zhao YM (2002) The important understanding for skarn deposits. *Miner Depos* 21:113–120 (in Chinese)
- Hou T, Zhang ZC, Pirajno F et al (2014) Geology, tectonic settings and iron ore metallogenesis associated with submarine volcanism in China: an overview. *Ore Geol Rev* 57:498–517
- Han BF, Guo ZJ, Zhang ZC et al (2010) Age, geochemistry, and tectonic implications of a late Paleozoic stitching pluton in the North Tian Shan suture zone, western China. *Geol Soc Am Bull* 122:627–640
- Xiao WJ, Huang BC, Han CM et al (2010) A review of the western part of the Altai: a key to understanding the architecture of accretionary orogens. *Gondwana Res* 18:253–273
- Jiang ZS, Zhang ZH, Hou KL (2012) Geochemistry and zircon U–Pb age of volcanic rocks from the Chagangnuoer and Zhibo iron deposits, western Tianshan, and the iron geological significance. *Acta Petrol Sin* 28:2074–2088 (in Chinese)
- Zhang ZH, Hong W, Jiang ZS et al (2014) Geological characteristics and metallogenesis of iron deposit in western Tianshan, China. *Ore Geol Rev* 57:425–440
- Wang YB, Jiang CY (2011) The chemistry and petrogenesis of Carboniferous rocks from Chagangnuoer iron deposits in western Tianshan, China. *Geol Sci Technol Inf* 30:18–27 (in Chinese)
- Sun JM, Ma ZP, Xu XY et al (2012) The formation epoch of the host wall rock of the Beizhan iron deposit in West Tianshan Mountains of Xinjiang and its geological significance. *Geol Bull Chin* 31:1973–1982
- Zhang ZH, Hong W, Jiang ZS et al (2012) Geological characteristics and zircon U–Pb dating of volcanic rocks from the Beizhan iron deposit in western Tianshan Mountains, Xin Jiang, NW China. *Acta Geol Sin* 86:737–747
- Xiao WJ, Windley BF, Badararch G et al (2004) Palaeozoic accretionary and convergent tectonics of the southern Altai: implications for the growth of central Asia. *J Geol Soc Lond* 161:1–4
- Xiao WJ, Han CM, Yuan C et al (2008) Middle Cambrian to Permian subduction-related accretionary orogenesis of North Xinjiang, NW China: implications for the tectonic evolution of Central Asia. *J Asian Earth Sci* 32:102–117
- Liu W, Liu XJ, Xiao WJ (2012) Massive granitoid production without massive continental-crust growth in the Chinese Altay: insight into the source of granitoids using integrated zircon U–Pb age, Hf–Nd–Sr isotopes and geochemistry. *Am J Sci* 312:629–684
- Gao J, Long LL, Klemd R et al (2009) Tectonic evolution of the South Tianshan orogen and adjacent regions, NW China: geochemical and age constraints of granitoid rocks. *Int J Earth Sci* 98:1221–1238
- Charvet J, Shu LS, Laurent-Charvet S et al (2011) Palaeozoic tectonic evolution of the Tianshan belt, NW China. *Sci Chin Earth Sci* 54:166–184

38. Gao J, Li MS, Xiao XC et al (1998) Paleozoic tectonic evolution of the Tianshan Orogen, northwestern China. *Tectonophysics* 287:213–231
39. Li JL, Su W, Zhang X (2009) Zircon Cameca U–Pb dating and its significance for granulite-facies granitic gneisses from the west Awulale Mountains, West Tianshan. *Geol Bull Chin* 28:1852–1862 (in Chinese)
40. Wang B, Shu L, Cluzel D et al (2007) Geochemical constraints on Carboniferous volcanic rocks of the Yili Block (Xinjiang, NW China): implication for the tectonic evolution of Western Tianshan. *J Asian Earth Sci* 29:148–159
41. Zhu YF, Zhou J, Guo X (2006) Petrology and Sr–Nd isotopic geochemistry of the Carboniferous volcanic rocks in the western Tianshan Mountains, NW China. *Acta Petrol Sin* 22:1341–1350 (in Chinese)
42. Song SG, Su L, Li XH et al (2010) Tracing the 850 Ma continental flood basalts from a piece of subducted continental crust in the North Qaidam UHPM belt, NW China. *Precambrian Res* 83:805–816
43. Liu YS, Hu ZC, Zong KQ et al (2010) Reap praisement and refinement of zircon U–Pb isotope and trace element analyses by LA-ICP-MS. *Chin Sci Bull* 55:1535–1546
44. Zong KQ, Liu YS, Gao CG et al (2010) In situ U–Pb dating and trace element analysis of zircons in thin sections of eclogite: refining constraints on the ultra high-pressure metamorphism of the Sulu terrane, China. *Chem Geol* 269:237–251
45. Williams IS (2001) Response of detrital zircon and monazite, and their U–Pb isotopic systems, to regional metamorphism and host-rock partial melting, Cooma Complex, southeastern Australia. *Aust J Earth Sci* 48:557–580
46. Rubatto D (2002) Zircon trace element geochemistry: partitioning with garnet and the link between U–Pb ages and metamorphism. *Chem Geol* 184:123–138
47. Möller A, O'Brien PJ, Kennedy A et al (2003) Linking growth episodes of zircon and metamorphic textures to zircon chemistry: an example from the ultra high temperature granulites of Rogaland (SW Norway). *Geol Soc Lond Spec Publ* 220:65–81
48. Pearce JA, Robinson PT (2010) The Troodos ophiolitic complex probably formed in a subduction initiation. *Gondwana Res* 18:60–81
49. Sun SS, McDonough WF (1989) Chemical and isotopic systematics of ocean basalt: implications for mantle composition and processes. In: Saunders A D, Norry MJ (eds) *Magmatism of the Ocean Basins*. *Geol Soc Spec Publ* 42:323–345
50. Che Z, Liu L, Liu H et al (1996) Review on the ancient Yili rift, Xinjiang, China. *Acta Petrol Sin* 12:478–490 (in Chinese)
51. Xia LQ, Xu XY, Xia ZC et al (2004) Petrogenesis of Carboniferous rift-related volcanic rocks in the Tianshan, northwestern China. *Geol Soc Am Bull* 116:419–433
52. Xia LQ, Xia ZC, Xu XY et al (2004) Carboniferous Tianshan igneous province and mantle plume. *Geol Bull Chin* 23:903–910 (in Chinese)
53. Wang JB, Xu X (2006) Post-collisional tectonic evolution and metallogenesis in northern Xinjiang, China. *Acta Geol Sin* 80:23–32 (in Chinese)
54. Zhou MF, Robinson PT, Leshner CM et al (2005) Geochemistry, petrogenesis and metallogenesis of the Panzhihua gabbroic Layered intrusion and associated Fe–Ti–V oxide deposit, Sichuan Province, SW China. *J Petrol* 46:2253–2280
55. Muntener O, Kelemen PB, Grove TL (2001) The role of H₂O during crystallization of primitive arc magmas under uppermost mantle conditions and genesis of igneous pyroxenites: an experimental study. *Contrib Miner Petrol* 141:643–658
56. Grove TL, Elkins TL, Parman SW et al (2003) Fractional crystallization and mantle-melting control on calc-alkaline differentiation trends. *Contrib Miner Petrol* 145:515–533
57. Rapp RP, Watson EB (1995) Dehydration melting of metabasalt at 8–32 kbar implications for continental growth and crust-mantle recycling. *J Petrol* 36:891–931
58. Petford N, Atherton M (1996) Na-rich partial melts from newly underplated basaltic crust: the Cordillera Blanca Batholith, Peru. *J Petrol* 37:1491–1521
59. Reiners PW, Nelson BK, Ghiorso MS (1995) Assimilation of felsic crust by basaltic magma: thermal limits and extents of crustal contamination of mantle-derived magmas. *Geology* 23:563–566
60. Downes H, Dupuy C, Leyreloup AF (1990) Crustal evolution of the Hercynian belt of Western Europe: evidence from lower-crustal granulitic xenoliths (French Massif Central). *Chem Geol* 83:209–231
61. Niu YL, Zhao ZD, Zhu DC et al (2013) Continental collision zones are primary sites for net continental crust growth: a testable hypothesis. *Earth Sci Rev* 127:96–110
62. Chen JF, Zhou TX, Xie Z et al (2000) Formation of positive (Nd_T) granitoids from the Alata Mountains, Xinjiang, China, by mixing and fractional crystallization: implication for Phanerozoic crustal growth. *Tectonophysics* 328:53–67
63. Hu AQ, Jahn BM, Zhang GX et al (2000) Crustal evolution and Phanerozoic crustal growth in northern Xinjiang: Nd isotopic evidence: Part I. Isotopic characterization of basement rocks. *Tectonophysics* 328:15–51
64. Naslund HR, Henríquez F, Nyström JO et al (2002) Magmatic iron ores and associated mineralization: examples from the Chilean High Andes and Coastal Cordillera. In: Porter TM (ed) *Hydrothermal iron oxide copper gold and related deposits: a global perspective*. Porter Geosci Consult Publ, Adelaide, pp 207–228
65. Chai FM, Geng XX, Yang FQ et al (2014) The Abagong apatite-rich magnetite deposit in the Chinese Altay Orogenic Belt: a Kiruna-type iron deposit. *Ore Geol Rev* 57:482–497
66. Yuan T (2003) Contrast of geological characteristics between Motuoshala iron (manganese) deposit and Shikebutai iron deposit in West Tianshan Mountain of Xinjiang Autonomous Region. *Contrib Geol Miner Resour Res* 18:88–92 (in Chinese)
67. Liu F, Yang FQ, Li YH et al (2009) Trace element and rare earth element characteristics of apatite from Abagong iron deposit in Altay City, Xinjiang. *Miner Dep* 28:251–264 (in Chinese)
68. Pirajno F (2009) *Hydrothermal processes and mineral system*. Springer Press, Perth, p 1250
69. Veksler I V, Dorfman AM, Danyushevsky LV et al (2006) Immiscible silicate liquid partition coefficients: implications for crystal-melt element partitioning and basalt petrogenesis. *Contrib Miner Petrol* 152:685–702
70. Jiang FZ (1983) A discussion on genetic types and metallogenetic characteristics of the marine volcanic iron and/or copper deposits in China. *Miner Dep* 2:11–18 (in Chinese)
71. Wenzel T, Baumgartner LP, Konnikov EG et al (2002) Partial melting and assimilation of dolomitic xenoliths by mafic magma: the Ioko-Dovyren intrusion (North Baikal Region, Russia). *J Petrol* 43:2049–2074
72. Bruno J, Wersin P, Stumm W (1992) On the influence of carbonate in mineral dissolution: II. The solubility of FeCO₃ (s) at 25 °C and 1 atm total pressure. *Geochim Cosmochim Acta* 56:1149–1155
73. Stem CR, Huang WL, Wyllie PJ (1975) Basalt-andesite-rhyolite-H₂O: crystallization intervals with excess H₂O and H₂O-undersaturated liquidus surfaces to 35 kilobars, with implications for magma genesis. *Earth Planet Sci Lett* 28:189–196
74. Lentz DR (1999) Carbonatite genesis: a reexamination of the role of intrusion-related pneumatolytic skarn processes in limestone melting. *Geology* 27:335–338